Anharmonic interatomic potentials of diatomic and linear triatomic molecules studied by extended x-ray-absorption fine structure

Toshihiko Yokoyama, Kaori Kobayashi,* and Toshiaki Ohta
Department of Chemistry, Graduate School of Science, The University of Tokyo, 7-3-1 Hongo, Bunkyo-ku, Tokyo 113, Japan

Akito Ugawa
Institute for Molecular Science, Myodaiji, Okazaki, Aichi 444, Japan
(Received 28 July 1995; revised manuscript received 15 November 1995)

The first four cumulants of a radial distribution function of diatomic molecules and the first three cumulants for linear triatomic systems have been derived quantum statistically. These moments are directly related to the second- to fourth-order force constants of the chemical bond. The temperature dependence of extended x-ray-absorption fine structure spectra of diatomic Br_2 and linear triatomic $HgBr_2$, $HgCl_2$, $AuBr_2^-$, and $CuBr_2^-$ systems has experimentally been investigated not only for the single-scattering paths but for the multiple-scattering paths. The resultantly obtained cumulants have successfully given the force constants, which are found to be in good agreement with the vibrational data. The differences of the force constants between the gas and solid phases are found even for the molecular crystals of $HgBr_2$ and $HgCl_2$.

I. INTRODUCTION

Extended x-ray-absorption fine structure (EXAFS) spectroscopy has widely been utilized for structure analysis in various fields of science.[1] EXAFS contains information on local structures around x-ray-absorbing atoms and usually gives coordination numbers and interatomic distances. Recently, thermal motions have also become an attractive subject, which are given in higher-order moments of radial distribution functions. In the case of harmonic oscillators, a reduction factor for the amplitude part is multiplied, which is so called a Debye-Waller factor (the second-order moment). When anharmonicity cannot be neglected, the phase part of the EXAFS function is also affected, this leading to significant errors in the interatomic distances.[2] It was of great importance to establish an analysis method in the presence of anharmonicity, and now the cumulant-expansion technique[3] has been regarded as the most practical method in the case of moderately disordered systems, while for largely disordered systems, for instance, the splice method[4] has been proposed. Both techniques are free from modeling radial distribution functions, and especially the cumulant expansion method has widely been applied not only to bulk materials,[5] but also to surfaces.[6,7] It can conclusively be remarked that the analysis method for the anharmonicity or asymmetric distribution has been established and that anharmonicity no longer prevents us from reliable structural parameters, but allows us to obtain additional useful information.

The next step for further understanding of the disorder problem is to know the direct relationship between the interatomic potential and cumulants. In the case of harmonic oscillators, the second-order cumulants have been formulated quantum mechanically for Debye crystals[8] and simple molecules.[9] On the other hand, Yokoyama *et al.*[10] have estimated the anharmonic potentials of metals and ionic crystals by using classic Boltzmann distribution functions of diatomic systems. Recently Rabus[11] and Frenkel and Rehr[12] have derived quantum-mechanical formulas including third-order anharmonicity for a simple diatomic system. Although these formulas are quite useful and have actually been applied to practical polyatomic systems,[5–7] quantitative discussions using these formulas cannot be performed, because N-atom systems have $3N-6$ vibrational modes and cannot be described by a single frequency. Previous studies using the diatomic approach have, in this sense, focused only on semiquantitative or comparative force constants. Very recently, Fujikawa and Miyanaga[13] have extended the theory to a one-dimensional infinite chain including the third and fourth-order cumulants and have emphasized the importance of polyatomic treatments.

In the present study, we have derived the formulas of the cumulants of the radial distribution function for a linear triatomic system. In a triatomic molecule, both symmetric and antisymmetric stretching modes contribute to the cumulants and the polyatomic treatment is found to be essentially important. We have further measured and analyzed temperature-dependent EXAFS spectra of diatomic Br_2 (gas phase), linear triatomic $HgBr_2(g)$, $HgBr_2$(solid phase), $HgCl_2(g)$, $HgCl_2(s)$, $AuBr_2^-$ and $CuBr_2^-$. The anharmonic potentials have subsequently been determined from the obtained cumulants and compared to the reported values given by the vibrational studies, if applicable. This EXAFS study determines anharmonic potentials not only for linear triatomic systems, but also for a simple diatomic molecular system.

In Sec. II of this article, we first summarize the treatment of thermal averages in the quantum-statistical perturbation theory and the EXAFS formula based on the cumulant-expansion technique, and subsequently we present the first four cumulant expressions for the diatomic system and also the first three cumulants for linear triatomic systems including the second-nearest-neighbor (NN) shell. Section III deals with experimental details and gives the brief results of far-infrared spectra taken for $AuBr_2^-$ and $CuBr_2^-$. In Sec. IV the

results of the diatomic Br_2 system are provided, and then the triatomic systems are discussed in detail. Section V summarizes the present investigation.

II. THEORY

A. Thermal average within first-order perturbation theory

Let us first recall the formalism of thermal averages within quantum-statistical perturbation theory.[14] A quantum-mechanical Hamiltonian of the system H is assumed to be given by

$$H=H_0+H', \tag{1}$$

where H_0 is the nonperturbed Hamiltonian whose Schrödinger equation is solved exactly and gives eigenvalues E_n and eigenfunctions $|n\rangle$, and H' is the perturbed term. Let us define the function $f(\beta)$ as

$$e^{-\beta H_0}f(\beta)=e^{-\beta(H_0+H')}, \tag{2}$$

where $\beta=(k_BT)^{-1}$, k_B the Boltzmann constant, and T the temperature. Equation (2) corresponds to the density matrix of the system including the perturbation, and we will obtain the first-order expansion of Eq. (2). On differentiating Eq. (2) with β and subsequent integration, one can easily transform Eq. (2) to the following integral equation using $f(0)=1$:

$$f(\beta)=1-\int_0^\beta e^{\beta' H_0}H'\ e^{-\beta' H_0}f(\beta')d\beta'. \tag{3}$$

Solving the integral equation successively, one reaches the first-order approximation form of the density matrix, which is given by substituting $f(\beta')=1$ in the right-hand side of Eq. (3). A thermal average of a certain physical quantity $\langle M\rangle$ is given exactly using the density matrix

$$\langle M\rangle=\frac{1}{Z}\,\mathrm{Tr}\,M e^{-\beta(H_0+H')}, \tag{4}$$

where Z is the partition function of the system. The first-order approximation gives

$$\mathrm{Tr}\,M e^{-\beta(H_0+H')}\cong\mathrm{Tr}\,M e^{-\beta H_0}\times\left(1-\int_0^\beta e^{\beta' H_0}H'\ e^{-\beta' H_0}d\beta'\right) \tag{5}$$

and

$$\frac{1}{Z}=\frac{1}{\mathrm{Tr}\,e^{-\beta(H_0+H')}}\cong\frac{1}{Z_0}\left(1+\frac{1}{Z_0}\,\mathrm{Tr}\,e^{-\beta H_0}\int_0^\beta e^{\beta' H_0}H'\ e^{-\beta' H_0}d\beta'\right), \tag{6}$$

where Z_0 is the partition function of the nonperturbed system. On performing the integral using $|n\rangle$ and E_n for the nonperturbed system, one obtains

$$\langle M\rangle\cong\frac{1}{Z_0}\sum_n e^{-\beta E_n}\langle n|M|n\rangle+\frac{1}{Z_0}\sum_{n,n'}\frac{e^{-\beta E_n}-e^{-\beta E_{n'}}}{E_n-E_{n'}}\langle n|M|n'\rangle\langle n'|H'|n\rangle+\frac{\beta}{Z_0^2}\sum_n e^{-\beta E_n}\langle n|M|n\rangle\sum_{n'}e^{-\beta E_{n'}}\langle n'|H'|n'\rangle, \tag{7}$$

where in the case of $n=n'$ the 0/0 factor in the second term should be replaced as

$$\frac{e^{-\beta E_n}-e^{-\beta E_n'}}{E_n-E_{n'}}=-\beta e^{-\beta E_n}. \tag{8}$$

Equation (7) is the final representation which is applied to the following calculations of cumulants.

B. Basic formula of EXAFS

The thermal average of the EXAFS oscillation function $\chi(k)$ (k is the photoelectron wave number) for a single shell is described within the framework of the single-scattering and plane-wave approximations:[1]

$$\chi(k)=A(k)\mathrm{Im}[e^{i\phi(k)}\langle e^{2ikr}\rangle], \tag{9}$$

where r is the distance between the x-ray-absorbing and scattering atoms, $\phi(k)$ is the total phase shift, and $\langle\ \rangle$ denotes the thermal average. $A(k)$ is the real amplitude factor, which is given in a more definite form such that

$$A(k)=\frac{S_0^2N}{kR^2}\,f_{\mathrm{eff}}(k), \tag{10}$$

where N the coordination number, R the average interatomic distance, S_0^2 the intrinsic loss factor due to many-electron effects, and $f_{\mathrm{eff}}(k)$ the effective backscattering amplitude including the spherical-wave effect and a factor of the inelastic scattering loss of the photoelectrons implicitly.

In order to evaluate $\langle e^{2ikr}\rangle$, the cumulant-expansion method is often employed:[1,3]

$$\langle e^{2ikr}\rangle=\exp\left[2ikr_0+\sum_n\frac{(2ik)^n}{n!}\,C_n\right], \tag{11}$$

where r_0 is the distance at the potential minimum, which is usually a temperature-independent quantity, and the C_n's are the cumulants. A usual EXAFS analysis deals with the cumulants up to the third or fourth order, which are related to the moments of the distribution function such as

$$R=\langle r\rangle=r_0+C_1,\quad C_2=\langle(r-R)^2\rangle,\quad C_3=\langle(r-R)^3\rangle,\quad C_4=\langle(r-R)^4\rangle-3C_2^2 \tag{12}$$

and so forth. By analyzing experimental EXAFS spectra by means of well-established procedures, one obtains structural parameters such as N, R, C_2, C_3, and C_4.

Here we should mention the approximations in Eqs. (9) and (10), whereby the functions $A(k)$ and $\phi(k)$ are approximately excluded from the thermal average integral calcula-

tion. Basically, the interatomic distance, effective backscattering amplitude, and total phase shift should show some temperature dependences because the interatomic distance varies due to thermal expansion and the latter two functions depend on the distance due to the spherical-wave effect of the emitted photoelectron. This would give some errors in the cumulants determined by the EXAFS analysis. The order of the errors can roughly be estimated when we perform the first-order expansions for r, $f_{\rm eff}(k)$, and $\phi(k)$ with respect to δr (small displacement of r). As a result, one can find that the power of the moments derived from the effect is always one order greater than that of the corresponding principal term; namely, C_2 and C_3 include the errors of the orders of C_3/R and C_4/R, respectively. This means that the error should be mostly less than $\sim$5%. Moreover, as described later, we will analyze the temperature dependence of the cumulants, this allowing significantly more reductions of the error bars compared to those of the absolute values. Although the relative errors can hardly be estimated precisely, these should be roughly in a few percent order or less. For C_2, C_3, and C_4 the analysis, errors would be greater, which may originate from the poor background subtraction in the EXAFS extraction and so forth. Only for the average distance is such a correction sometimes required because of its much higher accuracy.[3]

C. First four cumulants of diatomic systems

The cumulants of diatomic systems were successfully evaluated quantum mechanically up to third order by Rabus[11] and Frenkel and Rehr.[12] Although the practical procedures of the derivations are somewhat different, both results are found to be exactly the same. Here we will derive the first four cumulants including the fourth-order force constant. Let us consider a diatomic system AB with masses M and m for atoms A and B, respectively. An interatomic potential of the diatomic systems $V(r)$ is in general described such that

$$V(r)=\tfrac{1}{2}\kappa_0(r-r_0)^2-\kappa_3(r-r_0)^3+\kappa_4(r-r_0)^4+\cdots, \tag{13}$$

where r_0 is the distance at the potential minimum, κ_0, κ_3, and κ_4 the force constants, and r_0, κ_0, κ_3, and κ_4 are assumed to be temperature independent. Defining the displacement x, vibrational frequency ω, and reduced mass μ as

$$x=r-r_0, \quad \omega=\sqrt{\frac{\kappa_0}{\mu}}, \quad \mu=\frac{Mm}{M+m}, \tag{14}$$

the Hamiltonians are given by

$$H_0=-\frac{\hbar^2}{2\mu}\frac{d^2}{dx^2}+\frac{1}{2}\mu\omega^2x^2, \quad H'=-\kappa_3x^3+\kappa_4x^4+\cdots, \tag{15}$$

and the partition function of the nonperturbed system Z_0 is expressed as

$$Z_0=\sum_n \exp\left[-\frac{E_n}{k_BT}\right]=\sum_n z^n=\frac{1}{1-z}, \tag{16}$$

where

$$z=\exp\left[-\frac{\hbar\omega}{k_BT}\right].$$

Here the zero-point energy is omitted for simplicity since the factors are canceled in the calculation of thermal averages.

For the calculation of the odd term C_1, the first and third terms in Eq. (7) vanish and only the second term gives a nonzero value. As Frenkel and Rehr[12] have already shown, C_1 is given as

$$C_1=\langle r-r_0\rangle=\langle x\rangle=\frac{1}{Z_0}\sum_n\sum_{n'}\frac{z^n-z^{n'}}{E_n-E_{n'}}\langle n|-\kappa_3x^3+\kappa_4x^4|n'\rangle\langle n'|x|n\rangle. \tag{17}$$

Recalling the well-known formulas for the displacement x of harmonic oscillators, one finds that the summation over n' gives nonzero values only in the cases of $n'=n\pm1$. The even x^4 terms therefore all vanish, and only the odd x^3 terms remain. Using

$$\langle n|x|n+1\rangle=\sqrt{n+1}\,\sigma, \quad \langle n|x^3|n+1\rangle=3(n+1)^{3/2}\sigma^3, \quad \sigma=\sqrt{\frac{\hbar}{2\mu\omega}}, \tag{18}$$

one consequently obtains

$$C_1=\frac{6\kappa_3(1-z)}{Z_0\hbar\omega}\sigma^4\sum_n(n+1)^2z^n=\frac{6\kappa_3}{\hbar\omega}\sigma^4B, \tag{19}$$

where

$$B=\frac{1+z}{1-z}.$$

For the even terms of C_2 and C_4, all the terms in Eq. (7) should be evaluated, while the odd term C_3 requires only the second term in Eq. (7). The consequent formulas are given as

$$C_2=\langle(r-R)^2\rangle\cong\langle x^2\rangle=\sigma^2B-6\kappa_4\sigma^6\left(\frac{2B^2}{\hbar\omega}+\frac{B(B^2-1)}{k_BT}\right), \tag{20}$$

$$C_3=\langle(r-R)^3\rangle\cong\langle x^3\rangle-3C_1C_2=\frac{4\kappa_3\sigma^6}{\hbar\omega}(3B^2-2), \tag{21}$$

$$C_4=\langle(r-R)^4\rangle-3C_2^2\cong\langle x^4\rangle-3C_2^2=-3\kappa_4\sigma^8\left(\frac{2B(5B^2-3)}{\hbar\omega}+\frac{3(B^2-1)^2}{k_BT}\right). \tag{22}$$

Note that C_1 is proportional to the leading term of C_2.

D. First three cumulants of linear triatomic systems

Let us next consider a linear triatomic system AB_2 with masses M and m for central atom A and terminal atoms B (each specified as $B1$ and $B2$ hereafter), respectively. The interatomic potential V can be written in a form

$$V=\tfrac{1}{2}\kappa_0\Delta r_1^2+\tfrac{1}{2}\kappa_0\Delta r_2^2+\kappa_{12}\Delta r_1\Delta r_2-\kappa_3\Delta r_1^3-\kappa_3\Delta r_2^3+\cdots, \tag{23}$$

where Δr_1 and Δr_2 are, respectively, the relative displacements of A-$B1$ and A-$B2$ with respect to the distance at the potential minimum and κ_0, κ_{12}, and κ_3 are the force constants. Here we neglect the force constant κ_4 and cross terms higher than second order, and we omit the bending modes for simplicity because of no contribution to the cumulants. In the case of a harmonic approximation, the normal coordinates q and frequencies ω are given as

$$q_1=-\sqrt{\frac{m}{2}}\,(\Delta r_1+\Delta r_2),\quad q_2=-\sqrt{\frac{\mu}{2}}\,(\Delta r_1-\Delta r_2),$$

$$\omega_1=\sqrt{\frac{\kappa_0+\kappa_{12}}{m}},\quad \omega_2=\sqrt{\frac{\kappa_0-\kappa_{12}}{\mu}}, \tag{24}$$

$$\mu=\frac{Mm}{M+2m}.$$

q_1 and ω_1 correspond to the symmetric stretching mode, while q_2 and ω_2 to the antisymmetric stretching.

The nonperturbed and perturbed Hamiltonians H_0 and H' are expressed as

$$H_0=-\frac{\hbar^2}{2}\frac{\partial^2}{\partial q_1^2}+\frac{1}{2}\,\omega_1^2q_1^2-\frac{\hbar^2}{2}\frac{\partial^2}{\partial q_2^2}+\frac{1}{2}\,\omega_2^2q_2^2 \tag{25}$$

and

$$H'=\frac{\kappa_3}{\sqrt{2m}}\left(\frac{q_1^3}{m}+\frac{3q_1q_2^2}{\mu}\right)+\cdots, \tag{26}$$

where the nonperturbed Schrödinger equation is exactly solved with the eigenvalue $E_{n,l}$:

$$E_{n,l}=n\hbar\omega_1+l\hbar\omega_2\quad (n,l=0,1,2,3\ldots). \tag{27}$$

In Eq. (27) the zero-point energies are similarly omitted. The partition function of the nonperturbed system is given by

$$Z_0=\sum_{n,l}\ \exp\left[-\frac{E_{n,l}}{k_BT}\right]=\sum_{n,l}\ z_1^nz_2^l=\frac{1}{(1-z_1)(1-z_2)}, \tag{28}$$

where

$$z_1=\exp\left[-\frac{\hbar\omega_1}{k_BT}\right],\quad z_2=\exp\left[-\frac{\hbar\omega_2}{k_BT}\right]. \tag{29}$$

Let us first derive the cumulants for the first NN shell, which are described using powers of relative displacements between central atom A and terminal atoms $B1$ and $B2$. Two equivalent first-NN bonds (A-$B1$ and A-$B2$) equally contribute to the cumulants, and hence the experimentally obtained C_2 corresponds to the average

$$C_2=\frac{1}{2}\,\{\langle(\Delta r_1-C_1)^2\rangle+\langle(\Delta r_2-C_1)^2\rangle\}=\frac{1}{2m}\,\langle q_1^2\rangle$$

$$+\frac{1}{2\mu}\,\langle q_2^2\rangle-C_1^2. \tag{30}$$

Since the last term of C_1^2 is neglected in the present order of the approximation, only the thermal averages of q_1^2 and q_2^2 should be calculated. Moreover, only the first term in Eq. (7) is required because of neglect of the fourth-order force constant. The resultant formula is easily given within the harmonic approximation:

$$C_2=\tfrac{1}{2}\sigma_1^2B_1+\tfrac{1}{2}\sigma_2^2B_2, \tag{31}$$

where

$$B_1=\frac{1+z_1}{1-z_1},\quad B_2=\frac{1+z_2}{1-z_2},$$

$$\sigma_1^2=\frac{\hbar}{2m\omega_1},\quad \sigma_2^2=\frac{\hbar}{2\mu\omega_2}. \tag{32}$$

One finds that both the symmetric and antisymmetric stretching modes contribute to C_2 for the first-NN shell.

Since the first and third terms in Eq. (7) vanish in the calculation of odd-order moments, the second term is a leading term for C_1 or C_3. From the definition, C_1 is given by

$$C_1=\frac{1}{2}\,\langle\Delta r_1+\Delta r_2\rangle=-\frac{1}{\sqrt{2m}}\,\langle q_1\rangle, \tag{33}$$

this apparently implying that the displacement only for the symmetric stretching mode contributes to C_1. Calculating the second term of Eq. (7), the final form of C_1 is expressed as

$$C_1=\frac{3\kappa_3}{\hbar\omega_1}\,\sigma_1^2\,[\sigma_1^2B_1+\sigma_2^2B_2]=\frac{3\kappa_3}{\kappa_0+\kappa_{12}}\,C_2. \tag{34}$$

Although only q_1 contributes to C_1, the resultant formula contains the term of the antisymmetric stretching mode through the perturbed Hamiltonian or, in other words, due to the phonon-phonon coupling between the symmetric and antisymmetric modes. One derives the resultant formula of C_3 in a similar manner as

$$C_3=\frac{1}{2}\,\{\langle(\Delta r_1-C_1)^3\rangle+\langle(\Delta r_2-C_1)^3\rangle\}\cong-\frac{1}{(2m)^{3/2}}\,\langle q_1^3\rangle-\frac{3}{2\mu\sqrt{2m}}\,\langle q_1q_2^2\rangle-3C_1C_2$$

$$=\frac{\kappa_3\sigma_1^6}{\hbar\omega_1}\,(3B_1^2-2)+\frac{9\kappa_3\sigma_1^2\sigma_2^4}{2\hbar\omega_1}\,(B_2^2-1)+\frac{9\kappa_3\sigma_2^6}{\hbar\omega_1(\sigma_2/\sigma_1)^2-4\hbar\omega_2(m/\mu)}\left(\frac{1}{2}\,B_2^2-\frac{2\omega_2}{\omega_1}\,B_1B_2+\frac{1}{2}\right). \tag{35}$$

For the second-NN shell, the cumulants can be calculated easily since we have already evaluated the thermal averages of q_1, q_1^2, and q_1^3. The resultant formulas are the following:

$$C_1=\langle \Delta r_1+\Delta r_2\rangle=-\sqrt{\frac{2}{m}}\,\langle q_1\rangle=\frac{6\kappa_3}{\hbar\omega_1}\,\sigma_1^2[\sigma_1^2B_1+\sigma_2^2B_2], \tag{36}$$

$$C_2=\langle(\Delta r_1+\Delta r_2-C_1)^2\rangle\cong\frac{2}{m}\,\langle q_1^2\rangle=2\sigma_1^2B_1, \tag{37}$$

$$C_3=\langle(\Delta r_1+\Delta r_2-C_1)^3\rangle\cong-\left(\frac{2}{m}\right)^{3/2}\langle q_1^3\rangle-3C_1C_2$$
$$=\frac{8\kappa_3\sigma_1^6}{\hbar\omega_1}\,[3B_1^2-2]. \tag{38}$$

Note that, although for both the diatomic system and the first-NN shell of the linear triatomic system C_1 is simply proportional to C_2 as seen in Eqs. (19) and (34), such a relationship cannot be expected for the second-NN shell of the triatomic system. These equations are employed in the following analysis of temperature dependence of EXAFS spectra obtained experimentally.

III. EXPERIMENTAL DETAILS

A. Vibrational spectra

$(n\text{-}C_4H_9)_4NAuBr_2$ and $(n\text{-}C_4H_9)_4NCuBr_2$ were prepared and purified according to the literature.[15,16] Although the frequencies of the symmetric and antisymmetric stretching modes have been reported for $CuBr_2^-$,[17] these may not be exactly the same as those of the present samples since the previous spectrum[17] was taken in a solution. We have thus carried out the measurements of far-infrared spectra of solid $(n\text{-}C_4H_9)_4NAuBr_2$ and $(n\text{-}C_4H_9)_4NCuBr_2$ to verify the antisymmetric stretching frequencies. The spectra were recorded with a Bruker IFS 113v spectrometer for a energy range of 60–650 cm^{-1} with a resolution of 1 cm^{-1}. A silicon bolometer (Infrared Lab.) was used as a detector. Crystalline samples were ground and mounted on a white-polyethylene disk of 1 mm thickness. For the correction of the spectra, an absorption spectrum of the blank disk was subtracted from the raw data.

The resonance frequencies for $AuBr_2^-$ were found at 255 and 76 cm^{-1}. The former is assigned to the antisymmetric stretching mode and the latter to the bending mode. The antisymmetric stretching frequency of 255 cm^{-1} is consistent with the reported value of 254 cm^{-1}.[15] For $CuBr_2^-$ the antisymmetric stretching and bending modes were found at 324 and 81 cm^{-1}, respectively. The value of 324 cm^{-1} is again in good agreement with the reported one of 322 cm^{-1}. These findings imply that the stretching frequencies reported in the literature are available not only for the antisymmetric mode, but also for the symmetric stretching one. The numerical values are summarized in Table I, together with the force constants κ_0 and κ_{12}.

TABLE I. Symmetric and antisymmetric stretching frequencies ω_1 and ω_2 and force constants κ_0 and κ_{12} of $HgBr_2(g)$, $HgCl_2(g)$, $AuBr_2^-$ and $CuBr_2^-$. A stretching frequency and a force constant of diatomic $^{79}Br^{81}Br$ are also given.

Sample	ω_1 (cm^{-1})	ω_2 (cm^{-1})	κ_0 (mdyn/Å)	κ_{12} (mdyn/Å^2)
Br_2[a]	323.2		2.459	
$HgBr_2$[b]	222	293	2.282	0.035
$HgCl_2$[c]	358	413	2.655	0.022
$AuBr_2^-$[d]	209	254	1.867	0.190
$CuBr_2^-$[e]	193	322	1.570	0.182

[a]Reference 18
[b]Reference 19
[c]Reference 20
[d]Reference 15
[e]Reference 17

B. EXAFS

Temperature dependence of EXAFS spectra was investigated at BL-10B (Ref. 21) of the Photon Factory in the National Laboratory for High Energy Physics (the ring energy of 2.5 GeV and the stored ring current of 350–250 mA). EXAFS spectra were recorded with the transmission

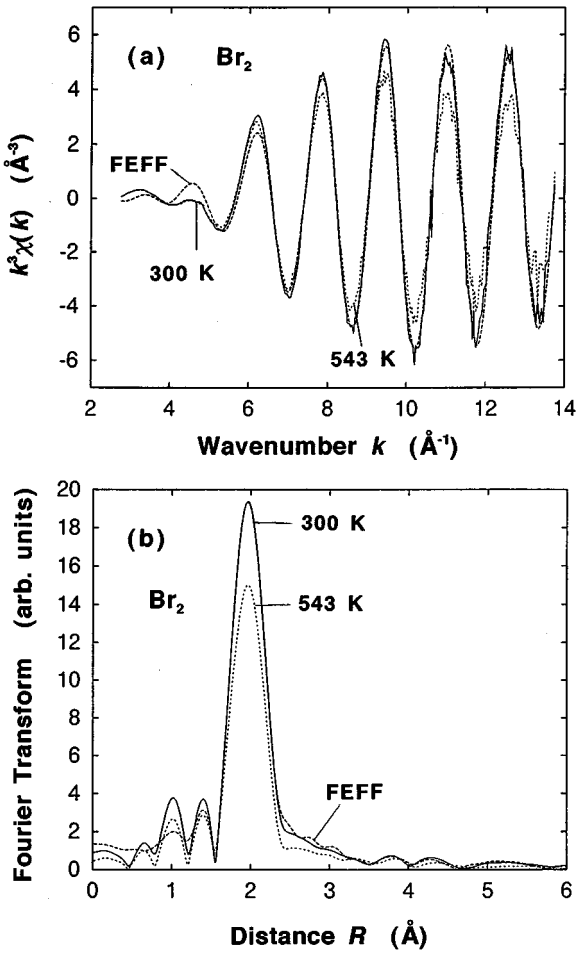

FIG. 1. (a) Br K-edge EXAFS oscillation functions $k^3\chi(k)$ and (b) their Fourier transforms of gaseous Br_2 at 300 K (solid line) and at 543 K (short-dashed line). The EXAFS function at 300 K calculated with FEFF6 is also depicted (long-dashed line).

TABLE II. Details of the present EXAFS analysis. N_I is the number of the independent data points, and Δk_{FT}, ΔR_{fit}, and Δk_{fit} are the employed ranges for Fourier transformation, Fourier filtering, and k-space fitting, respectively. In the refinements of FEFF, the curve-fitting analysis for $k^n\chi(k)$ has been performed with S_0^2, ΔE_0, and R as fitting parameters, while C_2 is fixed to the value calculated from the IR-Raman frequencies. In the analysis of temperature dependence (Temp.), the amplitude-ratio and phase-difference method has been adopted with ΔC_2, ΔR, and ΔC_3 as fitting parameters. For the second-NN shell, no curve-fitting analysis using FEFF parameters was conducted.

				FEFF		Temp.	
Sample	Shell	Δk_{FT} (Å^{-1})	ΔR_{fit} (Å)	Δk_{fit} (Å^{-1})	N_I	Δk_{fit} (Å^{-1})	N_I
$Br_2(g)$	first	2.7–13.75	1.6–2.4	3.5–13.5	6.1	6.0–13.5	4.8
$HgBr_2(g)$	first	2.5–11.5	1.5–2.5	3.0–11.0	6.1	6.0–11.0	4.2
	second	2.5–11.5	3.5–4.8			6.0–11.0	4.2
$HgCl_2(g)$	first	3.85–12.5	1.4–2.3	4.5–12.0	5.9	6.0–12.0	4.4
$HgCl_2(s)$	first	3.85–12.5	1.4–2.3	4.5–12.0	5.9	6.0–12.0	4.4
$AuBr_2^-$	first	3.1–15.9	1.75–2.5	4.0–15.5	6.5	6.0–15.5	5.5
	second	3.1–15.9	3.8–4.8			6.0–12.0	4.8
$CuBr_2^-$	first	2.5–16.0	1.7–2.3	3.5–15.5	5.6	6.0–15.5	4.6
	second	2.5–16.0	3.6–4.5			6.0–12.0	4.4

mode for a Br K edge for $Br_2(g)$ at 300 and 543 K, Hg L_{III} edges for $HgBr_2(g)$ at 656 and 838 K, $HgBr_2(s)$ at 58 and 300 K, $HgCl_2(g)$ at 618 and 747 K, and $HgCl_2(s)$ at 104 and 300 K, an Au L_{III} edge for $AuBr_2^-$ at 23 and 299 K, and a Cu K edge for $CuBr_2^-$ at 26 and 300 K. Commercially available Br_2, $HgBr_2$, and $HgCl_2$ were used without further purification. Ionization chambers were employed for the measurements of intensities of incident (I_0) and transmitted (I) x rays, which were filled, respectively, with N_2 for I_0 and Ar for I.

Solid samples were diluted with boron nitride, pressed to make disks with a diameter of 10 mm, and cooled down to the temperatures using a closed-cycle refrigerator. The absorption jumps at the edges were found to be less than 1.5 for all the solid samples, which implies fewer effects of higher harmonics at the present ring energy of 2.5 GeV. The sample temperature was monitored by an electric resistance of a Si diode placed closely to the sample disk.

For gaseous samples, solid $HgBr_2$ or $HgCl_2$ was put in a Pyrex-and-quartz cell with thin (~0.5 mm) quartz windows and the cell was subsequently evacuated and sealed, while gaseous Br_2 was just introduced to the same evacuated cell at ambient temperature. The cells were then heated up to the desired temperatures. These gases are known to be stable around the temperatures investigated. The total absorption coefficient of the gaseous samples including the quartz windows was less than 4 for the present energy range, this again indicating the lesser importance of higher harmonics.

IV. RESULTS AND DISCUSSION

A. Br_2

Let us first discuss the diatomic system of Br_2 prior to the triatomic systems. The EXAFS oscillation function $k^3\chi(k)$ was obtained with well-established procedures: pre- and post edge background subtractions and subsequent normalization with the absorption coefficients given in the literature.[1,22] The EXAFS functions $k^3\chi(k)$ taken at 300 and 543 K are shown in Fig. 1(a) together with the theoretically calculated one described below. Although strong oscillations due to Br-Br single scattering can be seen at both temperatures, the amplitude reduction at 543 K should be noted especially at a high-k region. This is based on the enhancement of thermal vibration at higher temperature. The EXAFS functions were subsequently Fourier transformed into r space, these being depicted in Fig. 1(b). Dominant features appearing at ~2 Å can be easily assigned to the single-scattering first-NN Br-Br shell.

In order to obtain structural parameters and also to verify the reliability of the present theoretical standards, calculations were performed using the FEFF6 program package.[23] FEFF6 includes *ab initio* calculations of atomic potentials to derive partial phase shifts and multiple-scattering EXAFS calculations using exact spherical-wave approaches. This calculation requires only a few undetermined parameters to reproduce EXAFS spectra, which are S_0^2 and ΔE_0. ΔE_0 is the shift of the edge energy, which has tentatively been chosen at the inflection point of the experimental data. For the calculation of the Br K-edge EXAFS of Br_2 at 300 K, the interatomic distance R of 2.2836 Å was taken from a rotational spectroscopic study[18] and the mean-square relative displacement C_2 of 0.002 07 Å was calculated from the vibrational frequency ω of 323.2 cm^{-1}.[18] C_3 was neglected for simplicity. Figure 1 includes the results of the FEFF6 calculation, which was obtained using optimized parameters of $S_0^2=1.05$ and $\Delta E_0=0.56$ (eV). Agreements between the experimental and theoretical spectra are found to be excellent.

A refinement of the interatomic distance was subsequently carried out by means of the curve-fitting analysis in k space. Details of the analysis parameters are summarized in Table II, together with those of triatomic systems described below. After the inverse Fourier transformation of the first-NN Br-Br shell of interest ($\Delta R_{fit}=1.6$–2.4 Å),[22] the extracted $k^3\chi(k)$ was fitted using the backscattering amplitude and the phase shift derived by the present FEFF6 calculation. Since the fitting k range is $\Delta k_{fit}=4$–13 Å^{-1}, the number of independent data points N_I is obtained to be ~5.6 using the well-known formula of $N_I=2\Delta k\Delta R/\pi+1$, while only the

three fitting parameters of S_0^2, R, and ΔE_0 were employed (C_2 was fixed to the values given by the Raman frequencies). The obtained distance R_{ex} is 2.286±0.010 Å, which is in good agreement with the reported value of 2.2836 Å, indicating a high reliability of the FEFF calculation. Here and hereafter the error bar includes both errors in the data and the fit.

The temperature dependence of the EXAFS spectra was finally analyzed by means of the amplitude-ratio and phase-difference methods. The logarithmic ratio of the amplitude part $\Gamma(k)=A(k)\exp[-2C_2k^2+2C_4k^4/3]$ between T_1 and T_2 can be expressed as

$$\ln\left[\frac{\Gamma(k,T_2)}{\Gamma(k,T_1)}\right]\cong -2[C_2(T_2)-C_2(T_1)]k^2 + \frac{2}{3}[C_4(T_2)-C_4(T_1)]k^4, \qquad (39)$$

and when the experimentally obtained logarithmic ratio is plotted as a function of k^2, ΔC_2 and ΔC_4 can be obtained through linear least-squares fittings with a second-order polynomial. Similarly, the difference of the phase part $\Psi(k)$ divided by k is written as

$$\frac{\Psi(k,T_2)-\Psi(k,T_1)}{k}=2[R(T_2)-R(T_1)] - \frac{4}{3}[C_3(T_2)-C_3(T_1)]k^2, \qquad (40)$$

and when the experimental left-side function in Eq. (40) is plotted versus k^2, the slope and y intercept lead to the differences in C_3 and R, respectively. Figure 2 shows the plots for the present Br_2 system (T_1=300 K and T_2=543 K). We used Δk_{fit}=6–13 Å^{-1}, this implying N_I=~4.6.

On the other hand, in the fitting procedure only one fitting parameter for the amplitude part (ΔC_2) and two fitting parameters (ΔR and ΔC_3) for the phase part were employed with the assumption of the same ΔE_0 and S_0^2 between 300 and 543 K. In the fitting procedure, one has to care about the correlation between S_0^2 and C_2. Since we investigate only the temperature dependence, S_0^2 does not vary essentially, but might be modified due to a poor estimation of the absorption edge jump. However, we have observed exactly the same edge jumps (discrepancy of less than 0.3%) between 300 and 543 K because we did not touch the sample cell during the continual EXAFS measurements. This implies that the error of the S_0^2 difference does not affect the estimated result of ΔC_2 since the major error should originate from poor background subtraction of the μ_0 spline function. Actually, one can see discrepancies between the experimentally obtained curves and the fitted lines, the former of which gives slight artificial oscillations. The resultant values are obtained from Fig. 2 to be ΔR=0.0022 Å, ΔC_2=0.001 24(6) Å^2, and ΔC_3=0.000 024(5) Å^3. Using the values of ΔC_2 and ΔC_3, the force constants κ_0 and κ_3 are evaluated as κ_0=2.43(10) (mdynÅ) and κ_3=1.5(3) (mdyn/Å^2). These values are consistent with the literature data of κ_0=2.459 (mdyn/Å) and κ_3=1.76 (mdyn/Å^2),[18] implying high accuracy of the present EXAFS analysis. Although in the present calculation we have employed ΔC_3 instead of ΔR for the calculation of κ_3 because of the greater reliability of ΔC_3, the estimated ΔR from the obtained κ_0 and κ_3 is 0.0023 Å, which is also in excellent agreement with the value of ΔR =0.0022 Å given independently from the phase analysis.

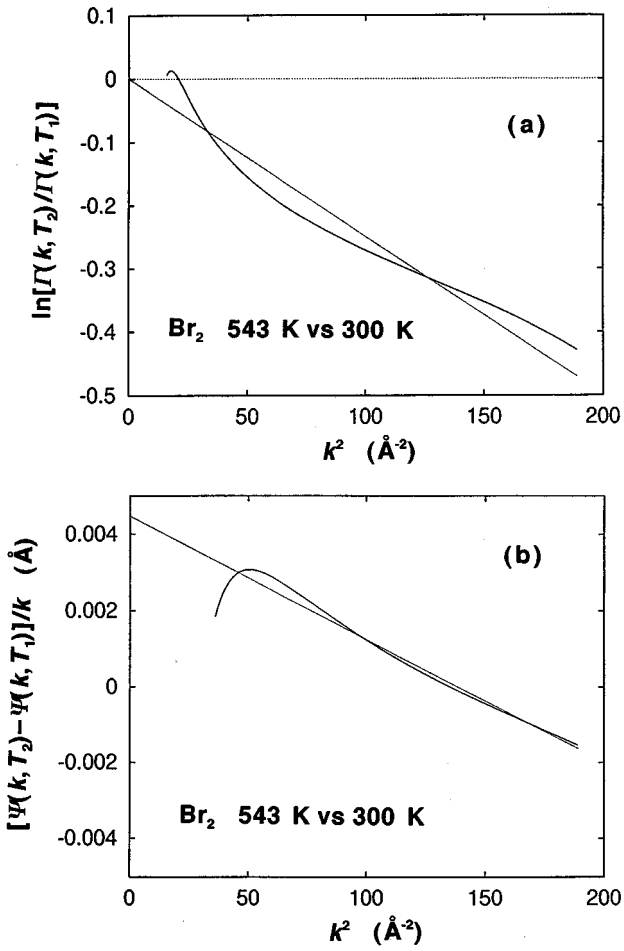

FIG. 2. (a) Logarithmic ratio of the amplitude functions and (b) phase difference divided by k as functions of k^2, for gaseous Br_2 between 300 and 543 K.

B. Triatomic systems

Experimental EXAFS functions $\chi(k)$ of the triatomic systems were obtained in a similar manner to the Br_2 case, and, as an example, the Hg L_{III} edge $k^2\chi(k)$ of gaseous $HgBr_2$ at 656 K is depicted in Fig. 3(a), and Fourier transforms of the triatomic systems studied are shown in Fig. 3(b) [$HgBr_2(g)$] and Fig. 4 [the other samples $HgCl_2(s)$ not shown]. Note that $k^3\chi(k)$ was employed for all the spectra except for $HgBr_2$. In all the Fourier transforms, the strong first-NN shells appear at ~2 Å and higher-shell contributions are also clearly seen around ~4 Å. Since no single-scattering contribution is expected around ~4 Å in the present cases where the central atoms of the triatomic systems is x-ray-absorbing atoms, these features should be attributed exclusively to the multiple-scattering paths. In order to give a detailed understanding of the whole feature, FEFF6 calculations were similarly performed for $HgBr_2(g)$, $HgCl_2(g)$, $AuBr_2^-$, and $CuBr_2^-$. In these four examples, the EXAFS functions could be described within one molecule even in the cases of the solids $(C_4H_9)_4NAuBr_2$ and $(C_4H_9)_4NCuBr_2$. In the cases of

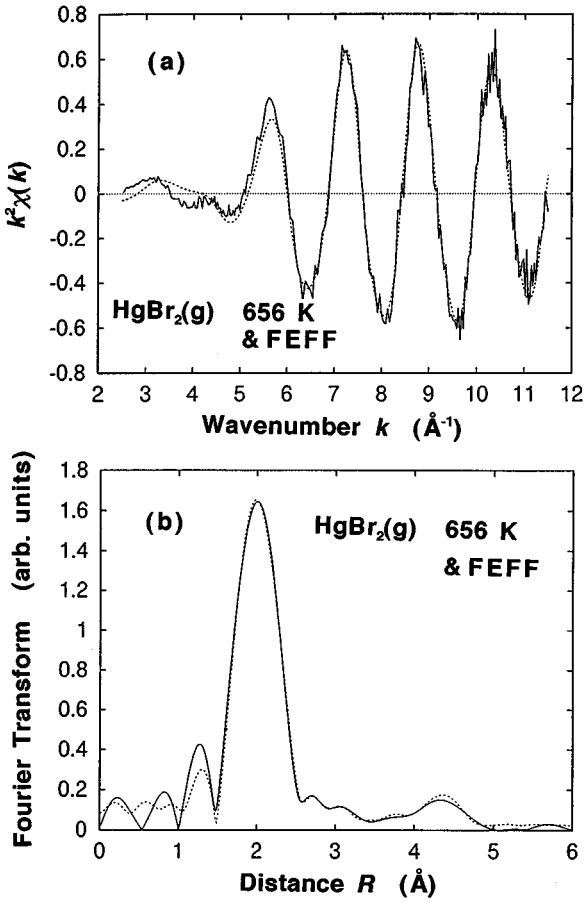

FIG. 3. (a) Hg L_{III}-edge $k^2\chi(k)$ and (b) its Fourier transform of gaseous $HgBr_2$ at 656 K (solid line), together with those calculated with FEFF6 (dashed line).

$HgBr_2(s)$ and $HgCl_2(s)$, neighbor molecules should also contribute to the EXAFS spectra and the FEFF simulations have not been carried out since these calculations are beyond the present purpose. Actually, the feature appearing at ~3 Å in the Fourier transform [Fig. 4(a)] can be ascribed to the intermolecular Hg-Br shell with $N=4$ and $R=3.23$ Å.[24]

In the cases of linear triatomic AB_2 systems, the total EXAFS function $\chi(k)$ is given by

$$\chi(k)=\chi_{\mathrm{I}}(k)+\chi_{\mathrm{II}}(k)+\chi_{\mathrm{III}}(k)+\chi_{\mathrm{IV}}(k), \tag{41}$$

where $\chi_{\mathrm{I}}(k)$ corresponds to the first-NN shell (single-scattering path A-B-A) and $\chi_{\mathrm{II}}(k)$, $\chi_{\mathrm{III}}(k)$, and $\chi_{\mathrm{IV}}(k)$ to the multiple-scattering paths, being, respectively, associated with A-$B1$-$B2$-A (double scattering), A-$B1$-A-$B2$-A (triple scattering), and A-$B1$-A-$B1$-A (triple scattering). Here higher-order multiple-scattering paths with longer distances were neglected. The results of the FEFF calculation are also given in Figs. 3 and 4. In these calculations, similarly to the case of the Br_2 calculation, the interatomic distances R were referred to from the structural studies in the literature[25–28] and the mean-square relative displacements C_2 were evaluated from the vibrational frequencies. The mean cubic relative displacements C_3 were neglected. The parameters to be optimized are thus S_0^2 and ΔE_0 for all the triatomic systems. These parameters are summarized in Table II. It is worthwhile mentioning that agreements between experimental and calculated spectra are excellent not only for the first-NN shell, but also for the multiple-scattering contributions around ~4 Å in spite of the employment of only two fitting parameters.

The interatomic distances for the first-NN shells were further refined by means of nonlinear least-squares routines, using effective backscattering amplitudes and phase shifts given by FEFF6. The fitting k ranges Δk_{fit} and the number of the independent data point, N_I, are summarized in Table II. The resultant values R_{ex} are given in Table III and those for $HgBr_2(g)$, $HgCl_2(g)$, $HgCl_2(s)$, $AuBr_2^-$, and $CuBr_2^-$ are found to be in good agreement with those of the diffraction studies.[25–29] The deviation between the present EXAFS and x-ray crystallographic studies[24] is, however, significant in the case of solid $HgBr_2(s)$. This might be because the x-ray-diffraction data were quite old and thus somewhat doubtful for the quantitative intramolecular distances. Actually, in solid $HgCl_2$ as well, the Hg-Cl distances given in Ref. 24 are 2.23 and 2.27 Å, which are much smaller than both the present finding and the new x-ray study.[29]

Figure 5(a) shows $k^2\chi(k)$, $k^2\chi_{\mathrm{I}}(k)$, $k^2\chi_{\mathrm{II}}(k)$, $k^2\chi_{\mathrm{III}}(k)$, and $k^2\chi_{\mathrm{IV}}(k)$ of $HgBr_2$ obtained from the present FEFF calculation, and their Fourier transforms (absolute values only) for the range of 3–6 Å are given in Fig. 5(b). This figure clearly shows that for the second-NN feature at ~4 Å the triple scattering $\chi_{\mathrm{III}}(k)$ is the most important and the double scattering $\chi_{\mathrm{II}}(k)$ should also be taken into consideration, while the triple scattering $\chi_{\mathrm{IV}}(k)$ can be neglected completely. Although the sidelobe of the strong first-NN feature still remains in the range around 4 Å, we will also neglect the contribution in the following temperature-dependent analysis because the first-NN shell might exhibit much weaker temperature dependence than the second-NN shell. The EXAFS function for the second-NN shell, $\chi_S(k)$, can thus be expressed as the sum of $\chi_{\mathrm{II}}(k)$ and $\chi_{\mathrm{III}}(k)$. Since the cumulants for the two scattering paths are exactly the same, this leads to

$$\chi_S(k)\cong\chi_{\mathrm{II}}(k)+\chi_{\mathrm{III}}(k)=\exp\{-2C_2k^2\}\mathrm{Im}[\exp\{i(2kR-\tfrac{4}{3}\,C_3k^3)\}\{A_{\mathrm{II}}(k)\exp\{i\phi_{\mathrm{II}}(k)\}+A_{\mathrm{III}}(k)\exp\{i\phi_{\mathrm{III}}(k)\}\}]$$

$$=A_S(k)\exp\{-2C_2k^2\}\sin(2kR-\tfrac{4}{3}\,C_3k^3+\phi_S(k)). \tag{42}$$

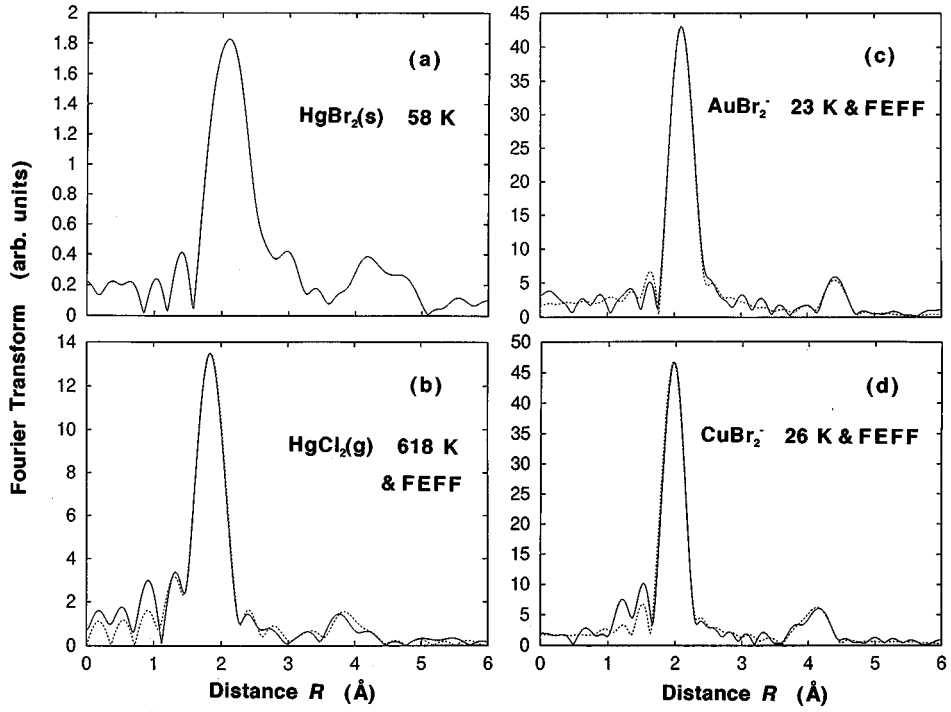

FIG. 4. Fourier transforms of (a) Hg L_{III} edge $k^2\chi(k)$ of $HgBr_2(s)$ at 58 K, (b) Hg L_{III} edge $k^3\chi(k)$ of $HgCl_2(g)$ at 618 K, (c) Au L_{III} edge $k^3\chi(k)$ of $AuBr_2^-$ at 23 K, and (d) Cu K edge $k^3\chi(k)$ of $CuBr_2^-$ at 26 K. Experimental data are given as solid lines. In (b), (c), and (d), those calculated with FEFF6 are also depicted as dashed lines.

Equation (42) implies that $\chi_S(k)$ can be analyzed in a similar manner to the case of the single-shell analysis.

Both the first- and second-NN shells have thus been analyzed by means of the amplitude-ratio and phase-difference methods which are well established for the single-shell EXAFS analysis. Details of the analysis parameters are given in Table II. Using Eqs. (39) and (40), the difference of the cumulants between two temperatures were evaluated. Figure 6 shows the logarithmic ratio of the amplitude functions and the phase difference divided by k of $HgBr_2(g)$ (T_1=656 K and T_2=838 K) as functions of k^2. The determined cumulants from the plots are summarized in Table IV, together with the results of the other materials. In the cases of $HgCl_2(g)$ and $HgCl_2(s)$, the second-NN shell could not provide reasonable plots as Figs. 2 and 6, possibly because with the increase in k, the backscattering amplitude of a chlorine atom is damped much more quickly than that of bromine, this leading to difficulty in the reliable analysis of the multiple-scattering paths. Only the results of the first-NN shells are thus presented for $HgCl_2$.

In order to evaluate κ_0 and κ_3 (we used C_3 for the estimation of κ_3), the cross term κ_{12} is required. Although the

TABLE III. Employed parameters in the FEFF calculations. S_0^2 and ΔE_0 were optimized so as to reproduce the experimental spectra most satisfactorily, while R_1 (1 denotes the first NN) and C_2 were taken, respectively, from the structural (Refs. 18, 24–29) and vibrational (Refs. 15, 17, 20) data. The distance R_{ex} is the refined value given by the curve-fitting analysis, namely, the distance determined by EXAFS. C_{21} is the mean-square relative displacement for the first-NN shell, while C_{22} and C'_{22} are for the second-NN shell, the paths of which correspond to A-$B1$-A-$B2$-A (or A-$B1$-$B2$-A) and A-$B1$-A-$B1$-A, respectively.

Sample	T (K)	S_0^2	ΔE_0 (eV)	R_1 (Å)	R_{ex} (Å)	C_{21} (Å^2)	C_{22} (Å^2)	C'_{22} (Å^2)
$Br_2(g)$	300	1.07	0.56	2.284[a]	2.286	0.002 07		0.008 28
$HgBr_2(g)$	657	0.92	−1.02	2.383[b]	2.374	0.004 07	0.007 96	0.015 82
$HgBr_2(s)$	58		−0.70	2.48[c]	2.443			
$HgCl_2(g)$	618	0.98	1.95	2.252[d]	2.250	0.003 43	0.006 74	0.013 72
$HgCl_2(s)$	104		−0.03	2.283[e]	2.299			
$AuBr_2^-$	23	0.93	8.52	2.385[f]	2.388	0.001 26	0.002 02	0.005 04
$CuBr_2^-$	26	0.83	4.84	2.226[g]	2.240	0.001 70	0.002 19	0.006 80

[a]Reference 18.
[b]Reference 25.
[c]Reference 24.
[d]Reference 26.
[e]Reference 29. Solid $HgCl_2$ is known to contain two different intramolecular Hg-Cl distances of 2.292 and 2.274 Å, and here the average value is given.
[f]Reference 27.
[g]Reference 28.

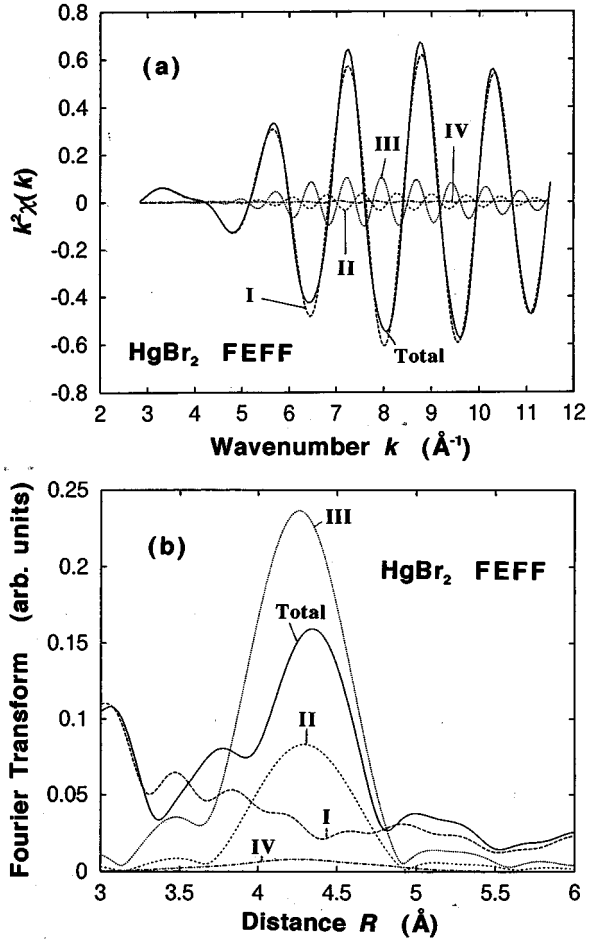

FIG. 5. (a) FEFF6 results of total $k^2\chi(k)$ (solid line), $k^2\chi_{\rm I}(k)$ (first-NN shell A-$B1$-A, long-dashed line), $k^2\chi_{\rm II}(k)$ (double-scattering second-NN shell A-$B1$-$B2$-A, short-dashed line), $k^2\chi_{\rm II}(k)$ (triple-scattering second-NN shell A-$B1$-A-$B2$-A, dotted line), and $k^2\chi_{\rm IV}(k)$ (triple-scattering second-NN shell A-$B1$-A-$B1$-A, dot-dashed line), and (b) their Fourier transforms.

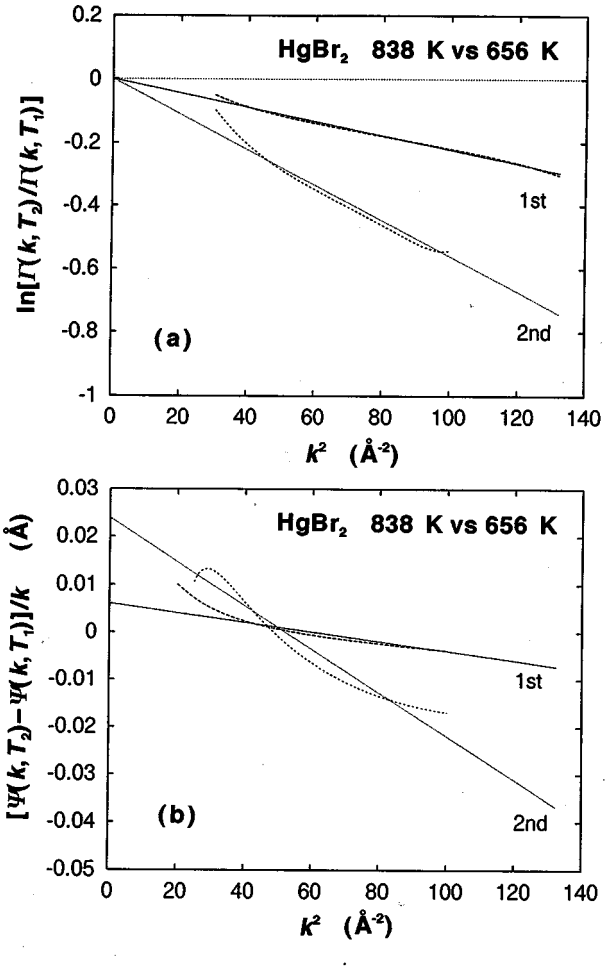

FIG. 6. (a) Logarithmic ratio of the amplitude functions and (b) phase difference divided by k as functions of k^2, for gaseous $HgBr_2$ between 656 and 838 K.

value is usually small enough to neglect compared to κ_0, the ratio κ_{12}/κ_0 was referred to from the vibrational data[15,17,19,20] in the present analysis. The numerical values of κ_0 and κ_3 are also given in Table IV. Although the values fluctuate somewhat between the results of the first- and second-NN shells, the finally estimated values with error bars are tabulated in Table V, together with the interatomic distances. Agreement of κ_0 between the present EXAFS and vibrational data is nonetheless fairly good, and we can expect that κ_0 can be obtained within error bars of less than $\pm 10\%$. It is interesting to compare the force constants κ_0 and κ_3 and the distance R

TABLE IV. The results of the analysis of temperature-dependent EXAFS of Br_2, $HgBr_2$, $HgCl_2$, $AuBr_2^-$, and $CuBr_2^-$. For the calculations of κ_0 of the triatomic systems, the ratio κ_{12}/κ_0 was taken from the vibrational data given in Table I.

Sample	Shell	T_2 (K)	T_1 (K)	ΔR (Å)	ΔC_2 (Å^2)	ΔC_3 (Å^3)	κ_0 (mdyn/Å)	κ_3 (mdyn/Å^2)
$Br_2(g)$	first	543	300	0.0022	0.001 24	0.000 24	2.43	1.5
$HgBr_2(g)$	first	838	656	0.0030	0.001 06	0.000 075	2.33	3.0
	second	833	656	0.0119	0.002 76	0.000 344	1.77	3.1
$HgBr_2(s)$	first	300	58	0.0131	0.001 76	0.000 166	1.39	4.7
$HgCl_2(g)$	first	747	618	0.0029	0.000 69	0.000 051	2.45	3.6
$HgCl_2(s)$	first	300	104	−0.0027	0.000 87	0.000 069	1.90	5.8
$AuBr_2^-$	first	299	23	0.0054	0.001 25	0.000 036	1.82	2.3
	second	299	23	0.0095	0.002 61	0.000 117	1.71	4.1
$CuBr_2^-$	first	300	26	0.0055	0.001 05	0.000 044	1.88	3.2
	second	300	26	0.0097	0.002 96	0.000 132	1.53	3.4

TABLE V. Comparison of interatomic distances R and force constants κ_0 and κ_3 between the present study and the literature.

	R (Å)		κ_0 (mdyn/Å)		κ_3 (mdyn/Å^2)
Sample	EXAFS[a]	Literature	EXAFS[a]	Literature	EXAFS[a]
$Br_2(g)$	2.285(10)	2.284[b]	2.4(1)	2.459[b]	1.5(2)
$HgBr_2(g)$	2.374(10)	2.383[c]	2.1(2)	2.282[i]	3.1(10)
$HgBr_2(s)$	2.443(10)	2.48[d]	1.5(2)		4.7(13)
$HgCl_2(g)$	2.250(10)	2.252[e]	2.5(2)	2.655[j]	3.6(12)
$HgCl_2(s)$	2.299(10)	2.286[f]	1.9(2)		5.8(17)
$AuBr_2^-$	2.388(10)	2.385[g]	1.8(2)	1.867[k]	3.2(10)
$CuBr_2^-$	2.240(10)	2.226[h]	1.7(2)	1.570[l]	3.3(10)

[a]This work.
[b]Reference 18.
[c]Reference 25.
[d]Reference 24.
[e]Reference 26.
[f]Reference 29.
[g]Reference 27.
[h]Reference 28.
[i]Reference 19.
[j]Reference 20.
[k]Reference 15.
[l]Reference 17.

between the gas and solid phases of $HgBr_2$ and $HgCl_2$. Larger κ_0 and smaller R in the gas phases indicate stronger intramolecular Hg-Br bonds than in the solid phase, and correspondingly anharmonicity in the gas phase is smaller because of smaller κ_3. Although $HgBr_2$ and $HgCl_2$ are regarded as molecular crystals in which intermolecular interaction is of a van der Waals force, the force constants have been revealed to vary significantly through the intermolecular interaction.

V. CONCLUSIONS

Since the vibrational frequency concerning heavy metals such as transition metal-ligand bonds is usually in the far-infrared region, vibrational studies seem sometimes difficult for the systems investigated. The temperature-dependent EXAFS technique is thus useful for studying dynamic properties of the chemical bonds for many systems such as surfaces, which can be hardly studied by means of far-infrared or Raman spectroscopy. Although the main purpose of the present work is a further fundamental understanding of EXAFS spectroscopy itself, the formalism and analysis method might be applicable to a practical use.

The present study has given the formulas of the first four cumulants for diatomic systems and the first three cumulants for linear triatomic systems by taking the thermal averages of moments of normal coordinates within quantum-statistical first-order perturbation theory. The cumulants are directly related to the force constants of the NN bond. In the case of the linear triatomic system, these are dependent on both the symmetric and antisymmetric stretching modes, this implying the importance of the polyatomic treatments.

The temperature dependence of EXAFS spectra of diatomic Br_2 and linear triatomic $HgBr_2$, $HgCl_2$, $AuBr_2^-$, and $CuBr_2^-$ systems has been analyzed. The theoretical standards FEFF6 yield excellent agreement with the experimental spectra for both the single- and multiple-scattering paths. The interatomic distances determined are consistent with recent structural studies within error bars of $\sim$0.01 Å. The second- and third-order force constants have been calculated from the cumulants obtained, which are also found to be in fairly good agreement with the ones obtained from the vibrational data. The difference of the force constants between the gas and solid phases has been clarified for $HgBr_2$ and $HgCl_2$, this finding corresponding to the difference of the interatomic distance.

ACKNOWLEDGMENTS

The present authors gratefully acknowledge H. Hamamatsu, S. Takenaka, and O. Endo for their help during the EXAFS measurements. We are also grateful to the Photon Factory staff, Professor M. Nomura, and Dr. N. Usami, who are in charge of Beamline 10B. This work has been carried out under the approval of Photon factory Program Advisory Committee (PF-PAC No. 94G226).

*Present address: Institute for Molecular Science, Myodaiji, Okazaki, Aich 444, Japan.

[1] See, for instance, *X-ray Absorption: Principles, Applications, Techniques of EXAFS, SEXAFS and XANES*, edited by D. C. Koningsberger and R. Prins (Wiley, New York, 1988).

[2] P. Eisenberger and G. S. Brown, Solid State Commun. **29**, 481 (1979).

[3] G. Bunker, Nucl. Instrum. Methods **207**, 437 (1983).

[4] Y. Ma and E. A. Stern, Phys. Rev. B **38**, 3754 (1988); I. Ono, T. Yokoyama, H. Sato, K. Kaneyuki, and T. Ohta, Jpn. J. Appl. Phys. **32**, 83 (1992); see also Ref. 1.

[5] See, for instance, T. Yokoyama and T. Ohta, Jpn. J. Appl. Phys. **29**, 2052 (1990); L. Tröger, T. Yokoyama, D. Arvanitis, T. Lederer, M. Tischer, and K. Baberschke, Phys. Rev. B **49**, 888 (1994).

[6] T. Yokoyama, H. Hamamatsu, Y. Kitajima, Y. Takata, S. Yagi, and T. Ohta, Surf. Sci. **313**, 197 (1994).

[7] L. Wenzel, J. Stöhr, D. Arvanitis, and K. Baberschke, Phys. Rev.

Lett. **60**, 2327 (1988); T. Lederer, D. Arvanitis, M. Tischer, G. Comelli, L. Tröger, and K. Baberschke, Phys. Rev. B **48**, 11 277 (1993).
[8] G. Beni and P. M. Platzman, Phys. Rev. B **14**, 1514 (1976).
[9] J. J. Boland and J. D. Baldeschwieler, J. Chem. Phys. **80**, 3005 (1984); *ibid*. **81**, 1145 (1984).
[10] T. Yokoyama, T. Satsukawa, and T. Ohta, Jpn. J. Appl. Phys. **28**, 1905 (1989).
[11] H. Rabus, Ph.D. thesis, Freie Universität Berlin, 1991.
[12] A. I. Frenkel and J. J. Rehr, Phys. Rev. B **48**, 585 (1993).
[13] T. Fujikawa and T. Miyanaga, J. Phys. Soc. Jpn. **62**, 4108 (1993); T. Miyanaga and T. Fujikawa, *ibid*. **63**, 1036 (1994).
[14] For instance, R. P. Feynman, *Statistical Mechanics* (Benjamin, Reading, MA, 1972).
[15] P. Braunstein and R. J. H. Clark, J. Chem. Soc. Dalton Trans. **1973**, 1845 (1973).
[16] M. Nilsson, Acta Chem. Scand. B **36**, 125 (1982).
[17] D. N. Waters and B. Basak, J. Chem. Soc. A **1971**, 2733 (1971).
[18] K. P. Huber and G. Herzberg, *Molecular Spectra and Molecular Structure IV: Constants of Diatomic Molecules* (Van Nostrand Reinhold, New York, 1979).
[19] W. Klemperer, J. Electrochem. Soc. **110**, 1023 (1963).
[20] W. Klemperer and L. Lindeman, J. Chem. Phys. **25**, 397 (1956).
[21] H. Oyanagi, T. Matsushita, M. Ito, and H. Kuroda (unpublished); M. Nomura (unpublished); M. Nomura and A. Koyama (unpublished).
[22] T. Yokoyama, H. Hamamatsu, and T. Ohta, EXAFSH, version 2.1, The University of Tokyo, 1993.
[23] J. J. Rehr, J. Mustre de Leon, S. I. Zabinsky, and R. C. Albers, J. Am. Chem. Soc. **113**, 5135 (1991); J. Mustre de Leon, J. J. Rehr, S. I. Zabinsky, and R. C. Albers, Phys. Rev. B **44**, 4146 (1991); J. Mustre de Leon, Y. Yacoby, E. A. Stern, and J. J. Rehr, *ibid*. **42**, 10 843 (1990); J. J. Rehr, R. C. Albers, and S. I. Zabinsky, Phys. Rev. Lett. **69**, 3397 (1992); J. J. Rehr, Jpn. J. Appl. Phys. **32**, 8 (1993).
[24] R. W. G. Wyckoff, *Crystal Structure*, 2nd ed. (Wiley, New York, 1963), Vol. 1, p. 307.
[25] *Structure Reports for 1985*, edited by G. Ferguson and J. Trotter (Reidel, Dordrecht, 1986), Vol. 52A, p. 352.
[26] K. Kashiwabara, S. Konaka, and M. Kimura, Bull. Chem. Soc. Jpn. **46**, 410 (1973).
[27] M. Melník and R. V. Parish, Coord. Chem. Rev. **70**, 157 (1986).
[28] M. Asplund, S. Jagner, and M. Nilsson, Acta Chem. Scand. A **37**, 57 (1983).
[29] V. Subramanian and K. Seff, Acta Crystallogr. B **36**, 2132 (1980).